

M. Micoulaut¹, S. Mechkov¹, D. Retraint², P. Viot¹ and M. François²

Granular gases in mechanical engineering: on the origin of heterogeneous ultrasonic shot peening

Granular gases in mechanical engineering

Received: date

Abstract The behavior of an ultrasonic shot peening process is observed and analyzed by using a model of inelastic hard spheres in a gravitational field that are fluidized by a vibrating bottom wall (sonotrode) in a cylindrical chamber. A marked heterogeneous distribution of impacts appears when the collision between the shot and the side wall becomes inelastic with constant dissipation. This effect is one order of magnitude larger than the simple heterogeneity arising from boundary collision on the cylinder. Variable restitution coefficients bring the simulation closer to the general observation and allows the investigation of peening regimes with changing shot density. We compute within this model other physical quantities (impact velocities, impact angle, temperature and density profile) that are influenced by the number N of spheres.

1 Introduction

It is well known that the introduction of residual compressive stresses in metallic components leads to reduce fatigue strength [1]. Therefore, many engineering techniques involve surface treatment to allow either surface hardening (by e.g. nitriding or vapor deposition) or fatigue life improvement [2] through laser shock peening or shot peening. For the latter, a high velocity stream of steel particles is projected at a material surface producing at and below it compressive residual stresses with a peak value being reached at some depth below the surface [3]. A particular mechanical treatment derived from conventional shot peening is called *ultrasonic shot peening*, ultrasonic is a reference to the frequency of vibration of the sonotrode (see below). It has received attention in

the recent years [4] since it could be a promising technique for obtaining surface treatment of metallic surfaces.

Here, a piezoelectric generator produces the vibration of a sonotrode that projects upon contact steel shot in a chamber closed by a cover which is the sample to be peened. The shot is usually made of small steel particles whose diameter is between 1 and 3 mm and the frequency is about 20kHz. Several parameters can also be changed, allowing one to control of the overall shot velocity and thus the shot peening intensity. Possible tuning parameters for optimizing the peening process include the shot diameter, the height of the chamber, the amplitude and/or the frequency of the sonotrode. Basic applications of this technology are found in automotive or aerospace industry.

If the performance of this process is closely related to the appropriate choice of parameters, it becomes necessary to understand how the peening intensity or the peening distribution on a given sample is affected by changes of mechanical or electrical characteristics of the system. Furthermore, as some of the physical quantities involved in the peening process are hard ¹ to measure in a real-time experiment (velocity, acceleration,...), mainly for safety reasons (the impact of steel beads are so strong that the chamber is a closed box), numerical simulation can be a powerful tool for investigating the influence of these quantities under various situations.

In parallel, there has been great activity during the last ten years in the study of granular gases [5; 6; 7]. In particular, systems of vibro-fluidized glass beads in a cylinder has some similarities with the device used for the shot peening [8; 9]. The main difference with the experimental setup used in ultrasonic shot peening is the absence of the cover and a lower frequency of vibration. In the latter series of experiments, it was shown that the inelastic sphere model provides an accurate description of microscopic quantities [10; 11] (local granular temperature, local mean velocity, local density, ...) which en-

¹Laboratoire de Physique Théorique de la Matière Condensée, Université Pierre et Marie Curie, Boite 121, 4, Place Jussieu, 75252 Paris Cedex 05, France

² Laboratoire des Systèmes Mécaniques et d'Ingénierie Simultanée, Université de Technologie de Troyes, BP 2060 -10010 Troyes Cedex, France

¹ Here, it is a real-time experiment.

courages us to perform a molecular dynamics of inelastic hard spheres.

The system is represented by a collection of inelastic hard spheres colliding with each other and with the boundaries (chamber, the shot, and sonotrode). For the sake of simplicity, collisions are first characterized by a constant normal coefficient of restitution. We perform an event-driven Molecular Dynamics that is as close as possible to the experimental setup by using the geometrical features of the chamber, sonotrode and the cover. In order to obtain an improved description of the model, we also consider a model of inelastic hard spheres where the restitution coefficient depends on the relative velocity of the impact.

Our results both theoretical and experimental show that the peening distribution on the sample is not homogeneous. The heterogeneity of the peening distribution is strongly influenced by the value of the particle-side wall coefficient of restitution c_w . This result goes far beyond the intuitive view that heterogeneity should simply result from the boundary collisions on the side walls. The increased energy dissipation along the side walls favors particle accumulation thus increasing the gas (shot) density on the border of the chamber. This leads to an increase of the impact frequency on the border of the sample. Within the model, we compute impact velocity and impact angle of the shot and show also a changing behavior with the shot density, ranging from the dilute Knudsen limit to a more dense situation where inter-particle collisions dominate. Both quantities display marked differences between the border and the center of the top wall (sample).

2 Inelastic hard sphere model

2.1 Simulation details

We first consider the model close to the experimental setup (see below). The cylinder has a radius of $R = 35 \text{ mm}$ which contains $N = 200$ hard spheres representing the shot of diameter 3 mm . The latter are subject to a constant gravitational force. The energy is supplied by vibrating the bottom wall following a symmetric saw-tooth profile with amplitude A and period T which mimics in the simulation the sinusoidal profile of the sonotrode². One should note that the choice of this profile has no major impact on the results[12], since the amplitude of the harmonic n of the saw-tooth profile falls as odd n^{-2} . We mention also that even though the electrical excitation of the sonotrode is sinusoidal, because

² By using a saw-tooth profile the time of a collision between a particle and the base is obtained analytically, whereas with a sinusoidal profile, the collision time is given by an implicit equation which requires a more expensive numerical computation.

of the elastic deformation of the sonotrode, the velocity applied to the shot is certainly not purely sinusoidal³.

The spheres collide inelastically and instantaneously with each other, with the cylindrical side walls, with the top wall and with the sonotrode. The corresponding constant coefficients of restitution are denoted c , c_w , c_b and c_t . The different collision rules are given by the following expressions:

$$\mathbf{v}'_{i,r} = \mathbf{v}_{i,r} - (1 + c_w)(\mathbf{v}_{i,r} \cdot \hat{\mathbf{r}}_{i,r})\hat{\mathbf{r}}_{i,r} \quad (1)$$

$$v'_{i,z} = v_{i,z} - (1 + c_b)(v_{i,z} - v_S) \quad (2)$$

$$v'_{i,z} = -(1 + c_t)v_{i,z} \quad (3)$$

$$\mathbf{v}'_{i,j} = \mathbf{v}_{i,j} \pm \frac{1 + c}{2}[(\mathbf{v}_j - \mathbf{v}_i) \cdot \hat{\mathbf{n}}]\hat{\mathbf{n}} \quad (4)$$

where the prime quantities denote the post-collisional quantities; $\mathbf{v}_{i,r}$ and $\hat{\mathbf{r}}_i$ is the unit position vector of particle i are the velocity and the position of the particle i in the horizontal plane respectively and c_w the normal coefficient of restitution for a collision between a sphere and the chamber. The particle-bottom (sonotrode) wall restitution coefficient c_b is first taken as unity which amounts to rescaling the amplitude of the vibration. v_S is the vertical velocity of the sonotrode; $v_{i,z}$ is the vertical component of the velocity of particle i and c_t the normal coefficient of restitution for a collision between a sphere and the cover; finally, $\mathbf{v}'_{i,j}$ denote the velocities of i or j particle, $\hat{\mathbf{n}}$ is the unit center-to-center vector between the colliding pair i and j and c is the normal coefficient of restitution for a sphere-sphere collision. One should note that there are two rules along the z axis (equations (2) and (3)) depending on which wall the spheres collide: bottom (sonotrode) or top (sample). Between collisions, the spheres follow parabolic trajectories due to the constant gravitational field (viscous damping with the air contained in the chamber is neglected).

The parameters of the model used in the simulation are obtained from experiment (Figure 1). The vibration frequency is 20 kHz and the amplitude of the sonotrode is $25 \mu\text{m}$. The chamber height is 40 mm . In the first part, we carry out most of the simulations with the restitution coefficients $c = c_t = 0.91$ corresponding to the usual experimental values for steel shot in the velocity range of interest [13] and leaving as an adjustable parameter only the side wall restitution coefficient c_w . This is in order to highlight the strong influence of the side-wall collisions on the impact heterogeneity. We stress however that the overall observed behavior of the model does not depend on the precise values given for c_t and c and several additional runs with different c_t and c have been performed to check the robustness of our conclusions. The stationary non-equilibrium state is achieved by a preliminary simulation of typically 5000 collisions per particle which

³ There can be a difference in amplitude of the sonotrode on the border and on the center.

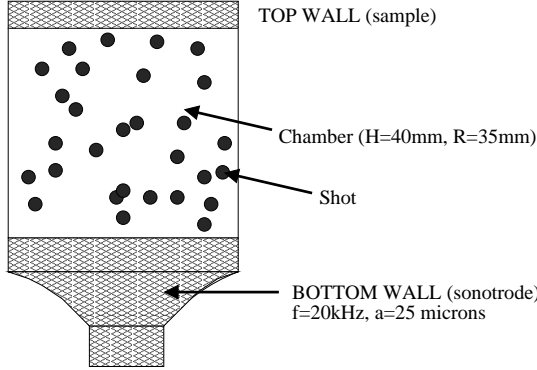


Fig. 1 Sketch of the experimental setup that is used as simulation box in the inelastic hard sphere model.

corresponds to a peening time of about $1ms$. The collision time estimated as $1\mu s$ from Hertz theory [14] is much lower. The statistical analysis of the quantities of interest has been accomplished for a total simulation time of $26s$ corresponding to 5×10^6 collisions.

2.2 Velocity dependent restitution coefficient

In a second part (section 3.2), the present model is made more realistic by taking into account velocity dependent normal restitution coefficients that depend on the normal impact velocity. This dependence is rather well known [15; 16; 17; 18; 19] and was first reported in the 1920's. Plastification under high velocities (typically when $v \geq 5 m.s^{-1}$) has also been reported. In the high velocity limit, experimental measurements suggest [14] a power-law behavior of the form: $c_N \propto v^{-1/4}$ whereas in the low velocity range, the deformations are supposed to be elastic and dissipation described by visco-elasticity [20; 21]. For the latter, it has been obtained [20] a slightly different power-law which is like $(1 - c_N) \propto v^{-1/5}$.

The behavior of restitution coefficients with respect to some easily measurable parameter is, however, a much deeper problem that can certainly not be encoded in the simple aforementioned power-laws. Experiments have indeed shown that c_N could depend on the sphere density [22], the sphere diameter or the thickness of the impacted surface [23], or even the impact angle [24; 25]. Beyond the details of a given material, studies on the restitution coefficient all suggest a generic threshold between a regime at low velocity and low dissipation where c_N depends weakly [26; 27] on the impact velocity, and a more dissipative regime induced by plasticity (or even fracturing) [28; 29].

Recently, simulations of inelastic hard spheres have been performed using variable restitution coefficients [30] and have shown the necessity of the latter to accurately describe experiments. Specifically, pressure effects as a function of the density of spheres could be recovered by simulation for a dilute and dense vibrated granular

Impacted material	i	c_0^i	v_0^i [cm/s]
Sonotrode (titanium)	b	0.91	1.2
Spheres (steel)	s	0.91	1.2
Sample (aluminum)	t	0.6	0.12
Side walls (aluminum)	w	0.6	0.12

Table 1 Parameters for the inelastic hard sphere model with variable restitution coefficient.

medium. It has been shown also that the unphysical clustering tendency was reduced with the use of velocity dependent restitution coefficients.

In section IIIB, we will use a threshold model for the normal restitution coefficient defined by:

$$c_N^i(v) = \begin{cases} c_0^i, & v \leq v_0^i, \\ c_0^i \left(\frac{v}{v_0^i} \right)^{-1/4}, & v \geq v_0^i \end{cases} \quad (5)$$

where v_0^i is a threshold velocity, c_0^i is the constant normal restitution coefficient at low velocity and $i = b, t, w, s$ following the nature of the impacted surface (bottom, top, wall, spheres). Parameters are given in Table I. One expects indeed that softer materials such as the aluminum side walls or the sample will have a lower threshold velocity and a lower c_0 as compared to the titanium sonotrode or the steel spheres.

Finally, we also use the simplest possible model to take into account the transverse dissipation that leads to a tangential restitution coefficient c_T . To our knowledge, only a very few studies have been reported on the subject (see however [31; 32]). The total loss of translational kinetic energy can usually be described by the total restitution coefficient $c = [c_N^2 \cos^2 \theta + c_T^2 \sin^2 \theta]^{1/2}$ where θ is the impact angle. Conservation of impulse and momentum and an additional condition of rolling prior to departure from the impacted surface leads to a value of $c_T = 5/7$ (the factor $5/7$ comes from the momentum of inertia). Here, it is assumed that the loss in kinetic energy mostly arises from the sphere rotation during the impact. One may also assume that slip continues throughout contact which will in this case lead to: $c_T = 1 - \mu(1 + c_N) \cot \theta$. But this would define an additional parameter μ corresponding to the Coulombic friction coefficient of the impacted surface. Experimental measurements of steel spheres bouncing on flat aluminum plates show [24] that the constant value of $c_T = 5/7$ is mostly valid at small impact angles and under certain conditions up to $\theta \simeq 55^\circ$. However, a more detailed analysis that should include the deformations and velocities associated with the elastic deformations of the surfaces is clearly beyond the scope and objectives of this paper. Since we are handling instantaneous impacts, effects of friction or peculiar material properties can only be taken into account via an *effective* velocity dependence of the restitution coefficients. Furthermore, we stress that this will not affect the general observed behavior with shot density.

3 Results

3.1 Origin of the impact heterogeneity

Figure 2 shows the different impact profiles that appear on the top wall of the chamber after 1 s simulation time for two different values of the side wall restitution coefficient c_w . For $c_w = c = c_t = 0.91$, one has an almost homogeneous distribution of impacts (Fig 2a) whereas heterogeneity sets in when c_w is lowered to 0.20 (Figure 2b). The present results have to be contrasted with the observed profiles obtained on the impacted aluminium sample after 1 s or on the sonotrode. It clearly shows that the inelastic sphere collision with the side wall are relevant for understanding the heterogeneous shot peening which is manifested by an increased impact number on the border of the sample. Nonelastic collisions on the side wall originate the impact profile that is experimentally observed (e.g. on the sonotrode (bottom wall), Fig 2c) and recovered from the simulation. The same profiles are obtained for the top wall with a similar impact frequency (see below).

The influence of the sphere-wall coefficient of restitution is quantitatively observed by monitoring the impact frequency per surface unit \mathcal{N} with respect to the radius R of the chamber (Fig. 3). It results that when the shot has a pure elastic collision on the side walls ($c_w = 1.0$), then the number of surface impacts slightly increases from the center to the radius of the chamber, whose values are in the range $\mathcal{N} = 0.6 - 0.8 \text{ impact.mm}^{-2}.s^{-1}$. When c_w decreases, a similar behavior is observed when the radial distance is lower than a typical value $R_0 \simeq 30 \text{ mm}$. For $R > R_0$ significant differences appear, e.g., for $c_w = 0.60$, the number of surface impacts is multiplied by almost a factor 10 between the center and the border of the cover and this increase is even more dramatic for the ultimate value of $c_w = 0.20$.

Intuitively, one expects that the impact distribution should be heterogeneous even in the case of elastic side wall collisions because of the lateral bounce on the cylinder wall. The simulation shows that this effect clearly seen from Fig. 3 when $c_w = 1.0$ is weak as compared to the effect arising from the decrease of c_w . Boundary collisions produce an increase of the surface impacts from $\simeq 0.5 \text{ mm}^{-2}.s^{-1}$ in the center to about $0.8 \text{ mm}^{-2}.s^{-1}$ on the border for elastic side wall collisions whereas the effect of lower side wall restitution coefficients (e.g. $c_w = 0.6$) leads to $\mathcal{N} = 1.8 \text{ mm}^{-2}.s^{-1}$ on the border of the top wall, compared to $\mathcal{N} = 0.25 \text{ mm}^{-2}.s^{-1}$ on the center. The present results do not depend crucially on the values taken for the other restitution coefficients as similar trends for the surface impact frequency are obtained for lowered c and c_t . For instance, when $c = c_t = c_w = 0.6$, the trend with R observed is rather close to the one displayed in Fig. 3 with $c_w = 0.6$, except that \mathcal{N} ranges now from 0.1 to $1.7 \text{ mm}^{-2}.s^{-1}$ between the center and the border of the sample.

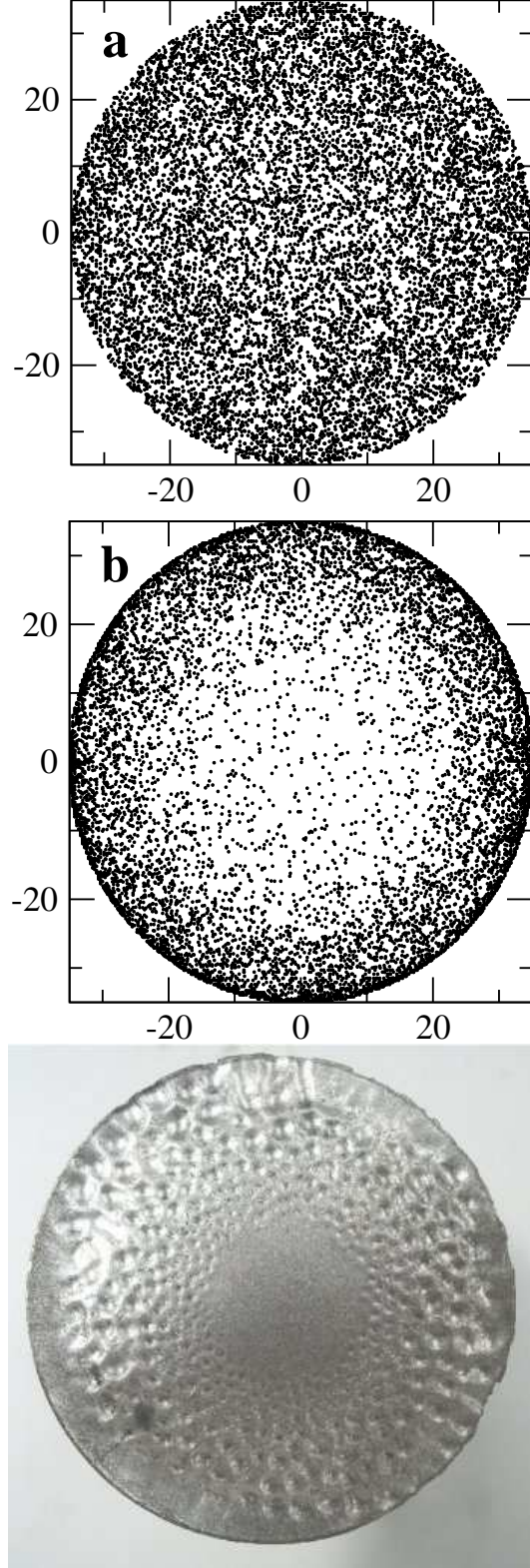


Fig. 2 Distribution of impacts on the top wall (sample). a) $c_w = 0.91$. b) $c_w = 0.20$. c) Sonotrode after several hours of use. See text for details.

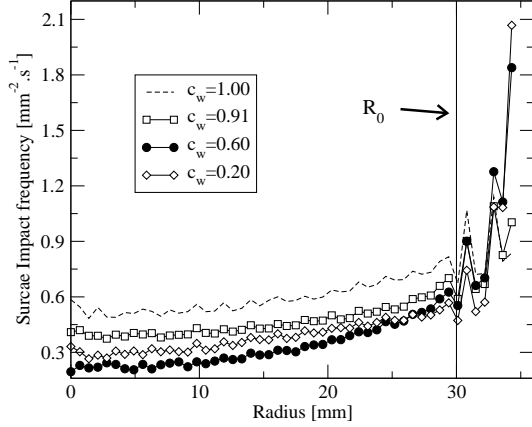


Fig. 3 Surface impact frequency with respect to the radial distance R for different side wall restitution coefficients c_w (symbols). The broken line corresponds to the pure elastic side wall collision ($c_w = 1$). The distance R_0 is used below (see text).

Beyond the numerical details, the origin of the heterogeneity becomes clear. With increased dissipation on the side walls, the spheres have a reduced velocity and are “adsorbed” on the side walls with an upward helicoidal trajectory arising from the impulse of the sonotrode. As a result, the density and the granular temperature (kinetic energy per particle) of the granular gas appear to be also strongly influenced by the dissipation.

3.2 Comparison with observation

Aluminum samples have been peened during 1 sec and the impact distribution displays a weak heterogeneity. The average roughness between the border and the center of the sample is respectively $4 \mu\text{m}$ and $7.4 \mu\text{m}$. In general, the obtained roughness reveals the degree of impact on a sample. It provides therefore an indirect evidence that more shot has been impacting the border. The heterogeneity can be quantified in a manner similar to Fig. 3 by sampling circularly the frequency of impacts \mathcal{N} per unit surface with respect to the radius of the sample. \mathcal{N} varies from 0.65 at the center of the sample to 0.95 on the border. The same tendency is obtained with rectangular sampling, i.e. one obtains $\mathcal{N} = 1.25 \pm 0.12$ at the center of the sample, and $\mathcal{N} = 1.66 \pm 0.39$ at the border. The presence of polymer adhesive stripes on the side walls that induce an increased dissipation, leads to a lowering of the respective impact frequencies, in harmony with the observed trends displayed in Fig. 3. Refinement of the measurements is currently under consideration.

3.3 Selective shot peening

Once the origin of the heterogeneity is identified, we investigate the effect of the sphere density (or sphere num-

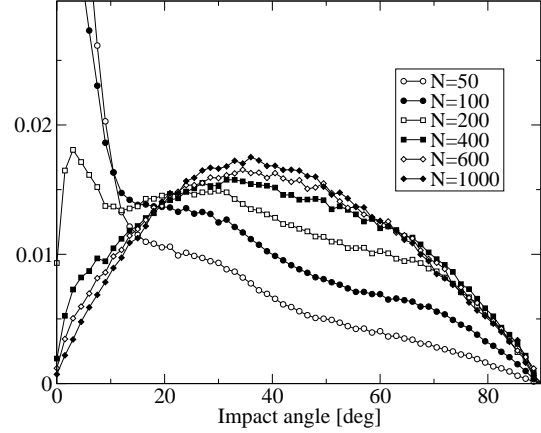


Fig. 4 Impact angle distribution on the top wall for different number of spheres N . All distributions are normalized to one.

ber N) in the chamber on the peening statistics. Within the inelastic hard sphere model using now the “realistic” restitution coefficients of Eq. (5), one has indeed the luxury to investigate features appearing with the progressive jamming of the system, starting from the very dilute limit, and characterize the deeper origin of the obtained profiles.

Figure 4 shows the impact angle distribution on the top wall (the sample) for various number of spheres. One can observe that the nature of the impacts can be very different following the very dilute ($N = 50$, density $\eta_0 = 3.25 \times 10^{-4} \text{ mm}^{-3}$) or more dense ($N = 1000$, $\eta_0 = 65.0 \times 10^{-4} \text{ mm}^{-3}$) situation. At low density, the impact is almost normal with a very sharp distribution centered around the impact angle $\theta = 0^\circ$. Here one sees that the spheres will mostly bounce back and forth between the top and the bottom walls with a rather small number of inter-particle collisions. As a result, the surface impact frequency \mathcal{N} with respect to the radius (Fig. 5) is rather flat and starts only to grow close to the side walls. With increasing N , these simple (mostly linear) trajectories tend to disappear as more and more sphere-sphere collisions are now involved. Finally, the distribution becomes very broad at high N and centered around $\theta = 35^\circ$ and there is not much difference between the system with $N = 600$ and $N = 1000$ spheres. Additional spheres do not change the obtained distribution. This shows also that in the more dense situation, normal impacts are very rare on the top wall, i.e. the probability of having $\theta = 0$ is almost zero. Noteworthy is the system with $N = 200$ spheres which displays an angular distribution that contains a reminiscent signature of the very dilute limit, i.e. showing a shallow peak around $\theta = 5^\circ$ which disappears when N is increased from 200 to 400. It suggests that in this intermediate situation, some spheres succeed in moving upwards through the granular gas without any sphere-sphere collision.

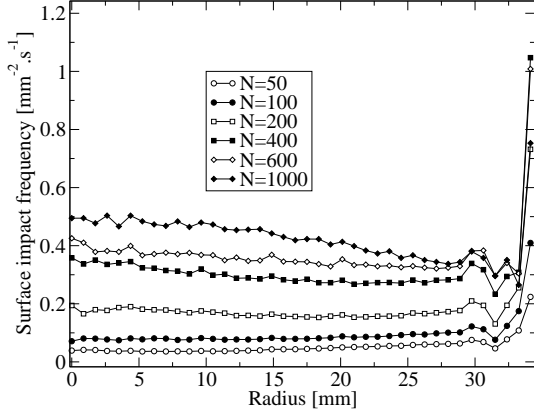


Fig. 5 Surface impact frequency \mathcal{N} on the top wall as a function of the radius of the chamber for different number of spheres.

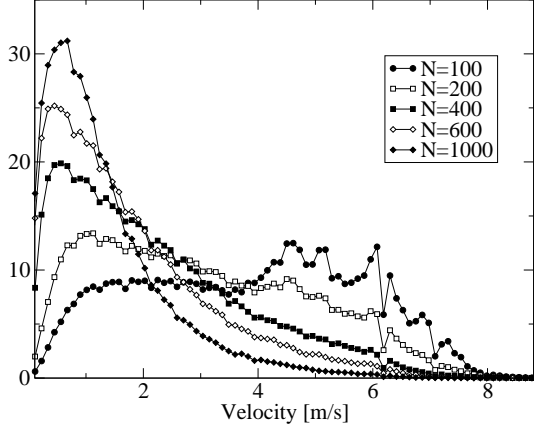


Fig. 6 Vertical impact velocity distribution on the top wall for different number of spheres N . All distributions are normalized to one.

Figure 5 shows an additional interesting feature which is the occurrence of a local order produced by the accumulation of the spheres on the side walls. With increasing N , more and more spheres are trapped on the side walls, similarly to the result of the constant restitution coefficient model (Figure 3). This produces an increased jamming in the vicinity of the side wall which does not allow other arriving spheres to reach it. As a result, these spheres will stay at a distance of the order of the diameter σ of the spheres. This is reflected in the quantity \mathcal{N} by an impact frequency peak at about $R = 30$ mm and even a secondary peak for high densities ($N = 600$ and $N = 1000$) between the latter value and the border of the sample.

Finally, we note that for a large number of spheres ($N = 1000$), the surface impact frequency decreases from the center of the sample to the first impact frequency peak at $R = 30$ mm. With the increased number of spheres, the impact velocity distribution (Fig. 6) refines

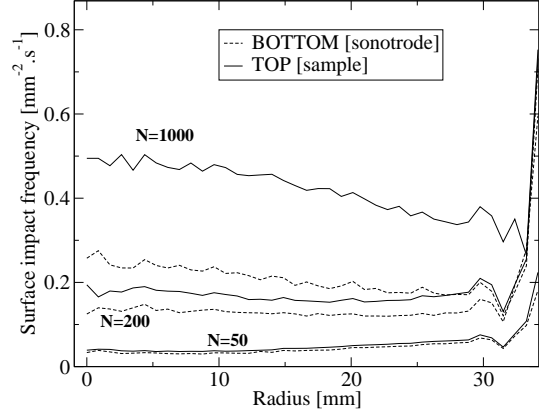


Fig. 7 Surface impact frequency \mathcal{N} on the top (solid lines, same as Fig. 3) and the bottom (broken lines) walls as a function of the radius of the chamber.

and converges to a Maxwell-Boltzmann-like distribution that can be fitted by $v_z \exp(-v_z^2)$ with a mean velocity that is of about 0.8 m/s and which is close to the measured velocities for this kind of system [13]. Note that for a small number of spheres, the impact velocity distribution is broad and ranges from 1 m/s up to large velocities of about 6 m/s corresponding to spheres that have been optimally accelerated by the sonotrode. Once the system densifies, the dissipation due to sphere-sphere collisions lowers the overall impact velocities.

A comparison between the surface impact frequency of the top and the bottom walls (Figure 7) shows that the impact regime can be rather different but still consistent with previous findings. For a very small number of spheres ($N = 50$), the result on the surface impact frequency is consistent with our previous findings, i.e. \mathcal{N} is identical between the top and the bottom, in agreement with the conclusion drawn from the impact angle distribution (Fig. 4), i.e. quasi-normal trajectories for the spheres which collide almost only between bottom and top. For an increased number of spheres, differences emerge which can become very pronounced as suggested by the value of the impact frequency on the center of sample for $N = 1000$. For the top wall, it is found $\mathcal{N} = 0.50$ mm².s⁻¹ whereas $\mathcal{N} = 0.26$ mm².s⁻¹ for the bottom wall, i.e. there is almost a factor of two between the two colliding walls. In order to infer the origin of the peening difference of the two surfaces, we have computed the mean velocity field for the system of inelastic spheres in the (R, z) plane. The field is averaged over the azimuthal angle and 5×10^6 collisions. Figure 8 shows the velocity field for the corresponding number of spheres used in Fig. 7. For $N = 200$, a toroidal convection roll is clearly present in which the particles flow, on average, up from the border and down the center. This kind of convection roll has been found both in simulations and experiment for open vibrated granular media [8; 10] at vibration frequencies of 50 Hz. The convec-

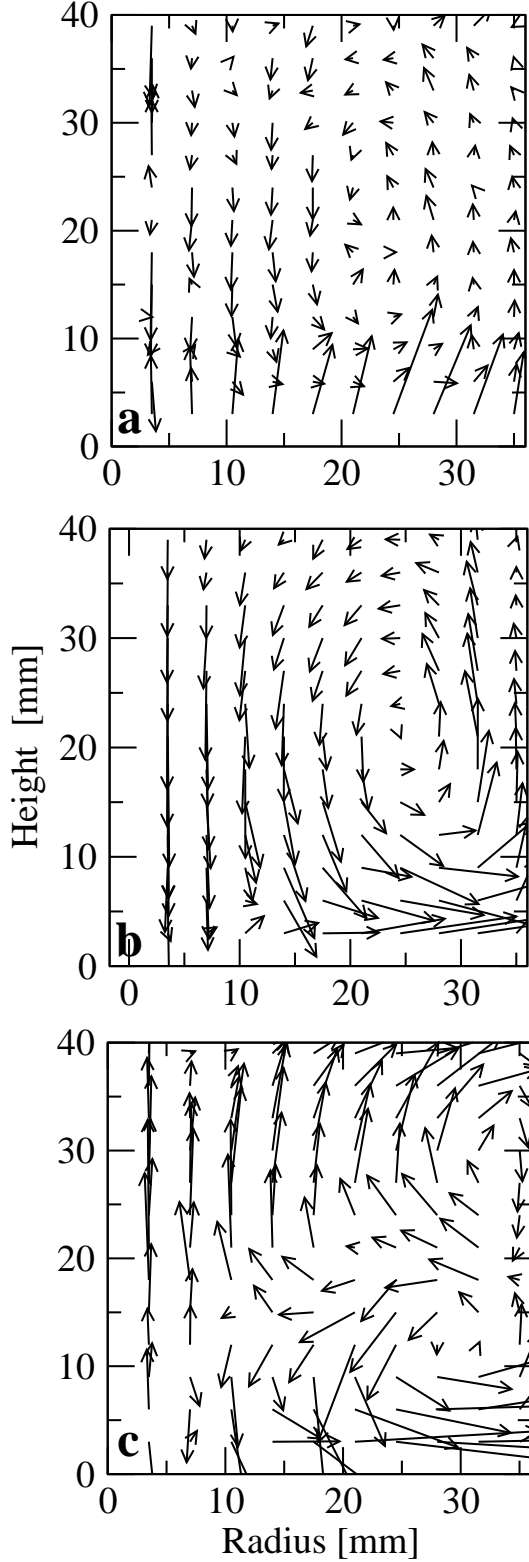


Fig. 8 Mean velocity field of the inelastic hard spheres in the (r, z) plane for three different numbers of spheres. a) $N=50$, b) $N=200$, c) $N=1000$.

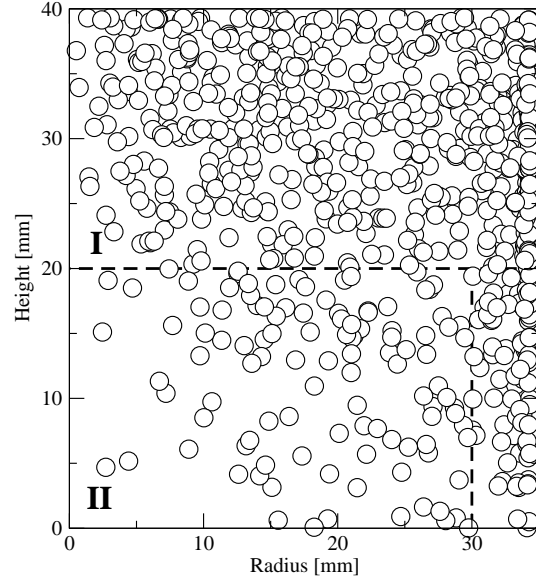


Fig. 9 A snapshot of the $N = 1000$ shot inside the chamber showing the density difference close to the top and close to the bottom wall. An average has been performed over the azimuthal angle, which explains observed overlaps discs. For clarity, the size of the spheres has been reduced. The broken lines serve to define the regions used in the discussion (see text) and in Fig. 10.

tion roll is maintained (but weaker by about an order of magnitude in intensity) for a lower number ($N = 50$) of spheres. However, one sees that for $N = 1000$, the convection roll breaks up and spheres flow from the side wall either upwards to hit the top of the chamber, or downwards to the sonotrode.

This tends to separate the chamber into two parts (Fig. 9). A first part (at $z > z_0$ with $z_0 \simeq 20$ mm) that connects to the top wall where the density is large ($\eta = 8.12 \times 10^{-3} \text{ mm}^{-3}$ and a packing fraction of 0.115). On the other hand, the lower part of the chamber corresponds to a much more dilute situation ($\eta = 4.87 \times 10^{-3} \text{ mm}^{-3}$ and a packing fraction of 0.069). Consequently, the upper impact angle distribution is radically different. The impact angle of the spheres bouncing on the more dense media at $z > z_0$ is very close to $\theta = 0^\circ$. This contrasts with the impact angle distribution of the upper part (Fig. 10).

4 Summary and conclusion

Simulations on inelastic hard sphere models using constant restitution coefficients clearly show that the inelasticity of the side-wall collisions plays a key role in the impact profile of the bottom and the top walls of a peening chamber. With increased dissipation, an increased heterogeneity of the impacts arising from the accumulation of the spheres on the side walls is found. The cor-

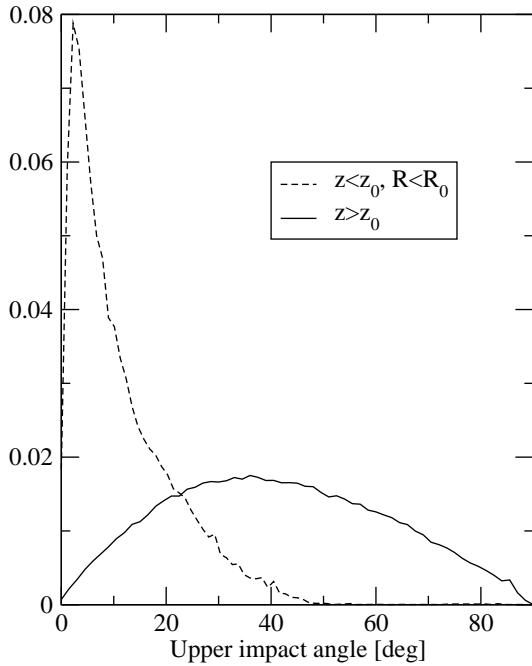


Fig. 10 Upper impact angle distribution for spheres belonging to region I ($z > z_0$, solid line, same as Fig. 4) and region II ($z < z_0$, $R < R_0$ broken line) for $N = 1000$. Both distributions are normalized to one.

responding surface frequency of impacts shows that the latter effect is one order of magnitude larger than the heterogeneity produced simple by oblique collisions arising from the side walls.

A model using variable restitution coefficients permits us to study in more detail the effect of the shot density (or number N of spheres) in the chamber. It shows that different peening regimes on the top wall take place with changing N that range from normal impacts for dilute granular gases, to oblique impacts with a well-defined mean impact velocity. Densification close to the side walls produces the occurrence of a local order at a distance of about the sphere diameter from the side walls.

These results suggest that elastic control of the side wall and a careful selection of the shot density will permit us to tune peening regimes for the shot and allow various kinds of surface treatments. The high density observed in the vicinity of the side walls is associated with a downwards helicoidal trajectory of the spheres. We believe that the use of a very rough surface on the side wall could lead to the reinjection of the spheres in the bulk. Further consideration in this direction along with deeper experimental characterization of the heterogeneity is currently under consideration.

Acknowledgments: Ongoing discussions and collaboration with Julian Talbot is gratefully acknowledged. LPTMC is Unité Mixte de Recherche du CNRS n. 7600. LASMIS is FRE CNRS 2719.

References

1. H. O. Fuchs and R. I. Stephens, *Metal Fatigue in Engineering* (John Wiley & Sons, Mississauga, Ontario, 1980).
2. J. P. Chu, J. M. Rigsbee, G. Banas, and H. E. Elsayed-Ali, *Mater. Sci. Engin. A* **260**, 260 (1999).
3. J. A. M. Ferreira, L. F. P. Boorrego, and J. D. M. Costa, *Fatigue, Fract. Engng. Mater. Struct.* **19**, 111 (1996).
4. J. Lu, P. Peyre, C. O. Nonga, A. Benamar, and J. F. Flavenot, *Proceedings of the 4th International Conference on Residual Stresses* 1154 (1994).
5. *Granular Gases*, edited by T. Pöschel and S. Luding (Springer, Berlin, 2001).
6. T. Pöschel and N. Brilliantov, *Granular Gas Dynamics* (Springer, Berlin, 2003).
7. I. Goldhirsch, *Annu. Rev. Fluid. Mech.* **35**, 267 (2003).
8. R. D. Wildman, J. M. Huntley, and D. J. Parker, *Phys. Rev. Lett.* **86**, 3304 (2001).
9. R. D. Wildman, J. M. Huntley, and D. J. Parker, *Phys. Rev. E* **63**, 061311 (2001).
10. J. Talbot and P. Viot, *Phys. Rev. Lett.* **89**, 064301 (2002).
11. J. Talbot and P. Viot, *Physica A* **317**, 672 (2002).
12. S. McNamara and J. L. Barrat, *Phys. Rev. E* **55**, 7767 (1997).
13. H. Chardin, 1996, PhD Thesis, Ecoles des Mines de Paris.
14. W. Goldsmith, *the theory and physical behaviour of colliding solids* (Dover Ed., London, 1990).
15. C. V. Raman, *Phys. Rev.* **12**, 442 (1918).
16. D. Tabor, *Proc. R. Soc. London* **192**, 247 (1948).
17. J. Okubo, *Sci. Rep. Temp. Tohoku. Univ. Ser. 1* **11**, 455 (1922).
18. J. P. Andrews, *Phil. Mag.* **9**, 593 (1930).
19. L. Labous, A. D. Rosato, and R. N. Dave, *Phys. Rev. E* **56**, 5717 (1997).
20. J. M. Hertzsch, F. Spahn, and N. V. Brilliantov, *J. Phys. II* **5**, 1725 (1995).
21. N. V. Brilliantov, F. Spahn, J. M. Hertzsch, and T. Pöschel, *Phys. Rev. E* **53**, 5382 (1996).
22. K. L. Johnson, *Contact Mechanics* (Cambridge University Press, Cambridge, 1985).
23. C. Zener, *Phys. Rev.* **59**, 669 (1941).
24. R. Sondergaard, K. Chaney, and C. Brennen, *J. Appl. Mech.* **57**, 694 (1990).
25. A. H. Karhaz, D. A. Gorham, and A. D. Salman, *Measurement. Sci. technol* **10**, 31 (1999).
26. N. V. Brilliantov and T. Pöschel, *Phys. Rev. E* **67**, 0611304 (2003).
27. T. Schwager and T. Pöschel, *Phys. Rev. E* **57**, 650 (1998).
28. A. Kharaz and D. Gorham, *Phil. Mag. Lett.* **80**, 549 (2000).
29. C. Thornton, *J. Appl. Mech.* **64**, 383 (1997).
30. S. McNamara and E. Falcon, *Phys. Rev. E* **71**, 031302 (2005).
31. R. M. Brach, *Int. J. Impact. Engng.* **7**, 37 (1988).
32. I. Goldhirsch, S. H. Noskovicz, and O. Bar-Lev, *Phys. Rev. Lett.* **95**, 068002 (2005).